



HAL
open science

Theoretical study on hydrogen solubility and diffusivity in the γ -TiAl L10 structure

Damien Connétable

► **To cite this version:**

Damien Connétable. Theoretical study on hydrogen solubility and diffusivity in the γ -TiAl L10 structure. *International Journal of Hydrogen Energy*, 2019, 44 (23), pp.12215-12227. 10.1016/j.ijhydene.2019.03.110 . hal-02134645

HAL Id: hal-02134645

<https://hal.science/hal-02134645>

Submitted on 20 May 2019

HAL is a multi-disciplinary open access archive for the deposit and dissemination of scientific research documents, whether they are published or not. The documents may come from teaching and research institutions in France or abroad, or from public or private research centers.

L'archive ouverte pluridisciplinaire **HAL**, est destinée au dépôt et à la diffusion de documents scientifiques de niveau recherche, publiés ou non, émanant des établissements d'enseignement et de recherche français ou étrangers, des laboratoires publics ou privés.




Open Archive Toulouse Archive Ouverte (OATAO)

OATAO is an open access repository that collects the work of some Toulouse researchers and makes it freely available over the web where possible.

This is an author's version published in: <https://oatao.univ-toulouse.fr/23845>

Official URL : <https://doi.org/10.1016/j.ijhydene.2019.03.110>

To cite this version :

Connétable, Damien  *Theoretical study on hydrogen solubility and diffusivity in the γ -TiAl L10 structure.* (2019) *International Journal of Hydrogen Energy*, 44 (23). 12215-12227. ISSN 0360-3199

Any correspondence concerning this service should be sent to the repository administrator:

tech-oatao@listes-diff.inp-toulouse.fr

Theoretical study on hydrogen solubility and diffusivity in the γ -TiAl L10 structure

Damien Connétable*

CIRIMAT, UMR 5085, CNRS INP UPS, ENSIACET, 4, allée Émile Monso, BP 44362, F-31030, Toulouse Cedex 4, France

ARTICLE INFO

Keywords:

TiAl
Hydrogen
DFT
Diffusion
Solubility
Intermetallic

ABSTRACT

The present work is a discussion on hydrogen solubility and diffusivity in the TiAl-L1₀ system using first-principles calculations. First, ground-state properties of the TiAl-L1₀ system are presented and discussed using elastic, phonon and thermal properties. They are compared with literature results. After having analyzed the geometry of L1₀ using the space-group theory, ten potential interstitial sites for hydrogen insertion were identified (among which the various octahedral and tetrahedral sites). After relaxation, only three configurations remained stable, but one site was significantly more stable than the others. The interactions between hydrogen and metal atoms are then described and analyzed by computing different quantities such as phonon properties, charge transfers, formation volumes and elastic dipoles. Diffusion mechanisms were then studied by analyzing the possible displacements at the atomic scale, and the diffusion coefficient of H atoms in TiAl was finally computed. Results show that H diffusion is strongly anisotropic.

Introduction

The development of new forming and manufacturing techniques, such as Spark Plasma Sintering (SPS) [1] or additive manufacturing (SLM, EBM) [2,3], has made it possible to use several materials (intermetallics and ceramics) that haven't been used for process reasons. Among the various classes of advanced materials, there has been a renewed interest in TiAl-based alloys. They have almost never been used, because of manufacturing issues (i.e., poor ductility at room temperature, problems in manufacturing processes). Today's new experimental opportunities make it possible to use them fewer machining steps. Hence the recent interest in TiAl alloys [1,2]. Indeed, they are lighter than Ti alloy systems and have equivalent elastic properties. TiAl alloys have been

widely considered as interesting structural materials for blades in high temperature applications. In-depth theoretical and experimental studies of their properties and behavior are rare, compared to what can be found for other unary [4–6] or binary systems [7,8].

Among failure modes, hydrogen embrittlement is a mechanism known to cause the ruin of metallic materials by reducing fracture toughness, increasing fatigue and leading to corrosion cracking. The mechanisms involved in hydrogen-induced interface weakening have always been worthy of interest [9–11], and the formation of sur-abundant vacancies (SAV) [12–14] can also explain hydrogen embrittlement in structural materials. However, these mechanisms do not fall directly within the scope of this paper. Before studying these complex mechanisms of interaction between hydrogen and the system it is important to understand the solubility of

* Corresponding author.

E-mail address: damien.connetable@ensiacet.fr.

<https://doi.org/10.1016/j.ijhydene.2019.03.110>

hydrogen in systems but also to predict its diffusion coefficient. In the literature, there are few studies on the solubility and diffusivity of hydrogen in TiAl-L1₀. Three theoretical works address H solubility [15–17]. Authors show that H insertion should happen in octahedral sites, but they do not indicate and describe which insertion sites. In terms of diffusivity data, Wang [17] only studied a few migration mechanisms but didn't compute diffusion coefficient values.

Few studies have addressed the mechanisms of hydrogen solubility and/or diffusivity in binary systems. Experiments have been mostly conducted in pure systems [4,18–21]. The present work is a complete study on hydrogen insertion and diffusion in the TiAl system. It includes a discussion on the interactions between hydrogen and metallic atoms, and a study on the diffusion mechanisms involved. Some contradictory values of H diffusivity were reported in the literature [22–25]. We will therefore compare and discuss our predictions in the light of these results.

To that end, the article is organized as follows. Section [Methodology](#) summarizes the method and calculations details. In [section Ground state properties of the TiAl-L1₀ structure](#), the ground states properties of the TiAl-L1₀ system are presented and discussed. The interactions between hydrogen and metal atoms are then investigated in [section Hydrogen solubility](#). In [section Hydrogen diffusivity](#), the diffusion mechanisms at the atomic scale are subsequently discussed. To conclude, hydrogen diffusion coefficients based on explicit formulas are presented.

Methodology

First-principles calculations were performed using the Vienna *ab initio* simulation package (VASP) [26]. The Perdew-Burke-Ernzerhof (PBE [27]) exchange and correlation functional were used. Spin polarized self-consistent Kohn-Sham equations were solved using projector augmented wave (PAW) pseudo-potentials [28] but no magnetism was found. The plane-wave energy cut-off was set to 600 eV, and $10 \times 10 \times 10$ Γ -centered Monkhorst-Pack meshes [29] were used to sample the first Brillouin zone (for $3 \times 3 \times 3$ super-cell). The lattice relaxations were introduced by using a conjugate-gradient algorithm. Forces applied on the ions and shapes of the system were relaxed.

The study of migration processes was conducted using CLIMB-NEB simulations [30] on $3 \times 3 \times 3$ super-cells. Transition states energies were computed with the same accuracy as stable position energies.

The vibrations were computed for stable and transition states in order to calculate attempt rates, Γ_{xy} and verify the stability of configurations. The *phonopy* package was used [31] to calculate inter-atomic force constants (IFC), vibration free energies and phonon band structures.

Ground state properties of the TiAl-L1₀ structure

The TiAl-L1₀ structure belongs to space-group 123 (P4/mmm, tP2). It is a tetragonal structure, where Ti atoms occupy the Wyckoff position 1a (0, 0, 0) and Al atoms the 1d position (1/2, 1/2, 1/2). The L1₀ structure can be depicted as an ordered face-

centered-tetragonal structure (in the z direction), where the two types of atoms alternate (002) atomic planes. It should be noted that this structure is very similar to a bcc structure, but it is not one. The closed phase, which is the TiAl-B2 phase, is not stable. The TiAl-L1₀ structure corresponds to a structure deformed in one direction (here the c axis). The structure is displayed in [Fig. 1](#).

The DFT values of the ground-state of the TiAl-L1₀ structure (lattice parameters and formation energies) are reported in [Table 1](#) and compared to theoretical and experimental results found in the existing literature (as well as to those of the reference phases). It can be noted that the lattice parameters and formation energies found experimentally [32,33] are in excellent agreement with our theoretical values and those of the literature [15,34]. The difference between PBE values and experimental values is small, about 0.5%. As expected, the lattice parameters of Mehl results [34], computed using the LDA functional, are slightly smaller than ours. But our results are similar to those presented by Chen [15] (GGA-PBE calculations).

The electronic band structure and density-of-states of TiAl are plotted in [Fig. 2](#). The system is found metallic with a high density of states ($n(\epsilon_f) \approx 1.8$ states per primitive cell). The s states of Al atoms hybridize with the s and p states of Ti atoms at low energy, in the range of $[-9; -3]$ eV. Near the Fermi level, ϵ_f , interactions are between the d states of Ti atoms and the p states of Al atoms.

The elastic properties of the TiAl-L1₀ and those of the reference states (Ti-hcp and fcc-Al) were afterwards computed using the finite displacements method as implemented in VASP (computed on the primitive cell, with $20 \times 20 \times 20$ k-meshes). Values found are compared to theoretical and experimental data in [Table 1](#). One first notes that the

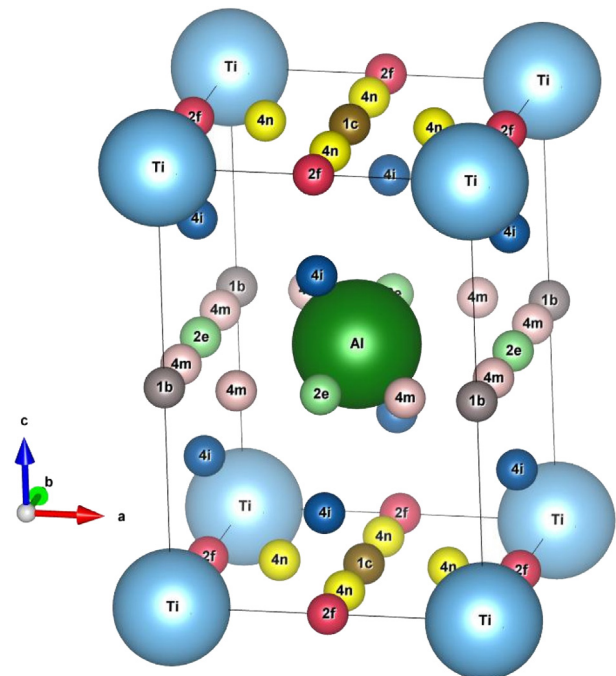


Fig. 1 – Schematic representation of the TiAl-L1₀ structure indicating all the interstitial positions that were tested.

Table 1 – Theoretical and experimental lattice parameters a_0 and c_0 (in Å), formation energies (E_f , in eV/atom), bulk (B , in GPa) and Young (E , in GPa) modulus, elastic constants (C_{ij} , in GPa) and Poisson coefficient (ν).

		a_0	c_0	E_f	B	ν	E
Ti (hcp)	this work	2.938	4.657	–	112	0.32	123
	GGA [20]	2.932	4.648	–	112	–	–
	exp.	2.945	4.544	–	112	–	–
TiAl (L1 ₀)	this work	3.999	4.076	–0.407	114	0.25	171
	GGA [15]	3.991	4.072	–0.407	–	–	–
	LDA [34]	3.90	4.05	–	127	0.24	198
	exp.	3.97–4.01 [32,33]	4.04–4.08 [32,33]	–0.392 [32]	110 [35]	–	183 [35]
Al (fcc)	this work	4.04	–	–	78	0.35	72
	exp [36].	4.05	–	–	78	–	–
		C_{11}	C_{33}	C_{44}	C_{66}	C_{12}	C_{23}
Ti (hcp)	this work	176	188	43	47	82	76
	GGA [20]	173	180	44	45	82	76
	exp [37].	172	180	44	45	82	76
TiAl (L1 ₀)	this work	171	172	112	64	88	85
	LDA [34]	188	190	126	100	98	96
	exp [35].	186	176	101	77	72	74
	[33]	187	182	109	81	75	75
Al (fcc)	this work	105	–	33	–	65	–
	exp [36].	106	–	31	–	65	–

elastic constants of reference states, C_{ij} , are reproduced with accuracy, see Ref. [20] and references cited for Ti and Ref. [36] for Al. Indeed, the discrepancy as low as $< 5\%$. For the bct TiAl structure, there are six independent constants, i.e. C_{11} , C_{33} , C_{44} , C_{66} , C_{12} and C_{23} . The values of C_{11} and C_{33} on one hand and those of C_{12} and C_{23} on the other are close to each-other. This can be explained by the low tetragonal nature of the system. It can also be noted that the values of C_{if} in TiAl-L1₀ and in Ti-hcp systems are very close. As expected, LDA simulations lead to smaller lattice parameters, shorter inter-atomic bonds, and therefore higher elastic constants. Our values agree well with theoretical (GGA) values found in the literature [15]. Please refer Chen's article [15] for a discussion on elastic constants. The Young modulus of the TiAl system is significantly higher than that of Ti-hcp, which also explains why this structure is interesting.

Finally, the phonon properties of TiAl-L1₀ were computed using the finite displacements approach on a $3 \times 3 \times 3$ supercell. From the forces calculated on super-cells with a reduced number of atomic displacements, IFCs were deduced using the *phonopy* package [31]. The plots of the phonon band structure and the projected density-of-states (calculated on

$40 \times 40 \times 40$ q -meshes grids) are displayed in Fig. 3. As expected, the motions in the acoustic dispersion curves are almost entirely associated with Ti atoms. The frequencies of Ti atoms are lower in energy than those of Al atoms, which is consistent with the fact that Al atoms are lighter than Ti atoms.

The dispersion curves around $q = \Gamma$, associated with the sound velocities, do not show any anomaly. Since the masses of Al and Ti atoms are close, there is no gap between the optical and the acoustic branches of the phonon modes in Fig. 3. From these phonon properties, the phonon free energy, the heat capacity (C_v) and then the zero-point energy of the H atom inserted in the system were computed. For instance, the Debye temperature, $\Theta_D = 559$ K, was computed from the heat capacity. This is in excellent agreement with the value found in the literature: 584 K.

Hydrogen solubility

The insertion of H atoms inside TiAl will now be analyzed. The present work focuses only on the solubility of H in the bulk.

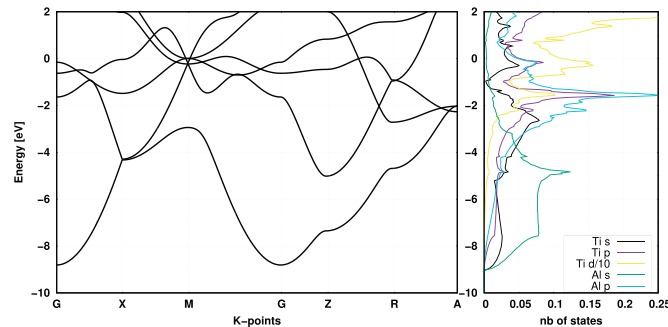


Fig. 2 – Electronic band structure along high symmetry k -points and electronic density-of-states of the TiAl-L1₀ structure, projected states on atoms. The Fermi level is set at 0eV.

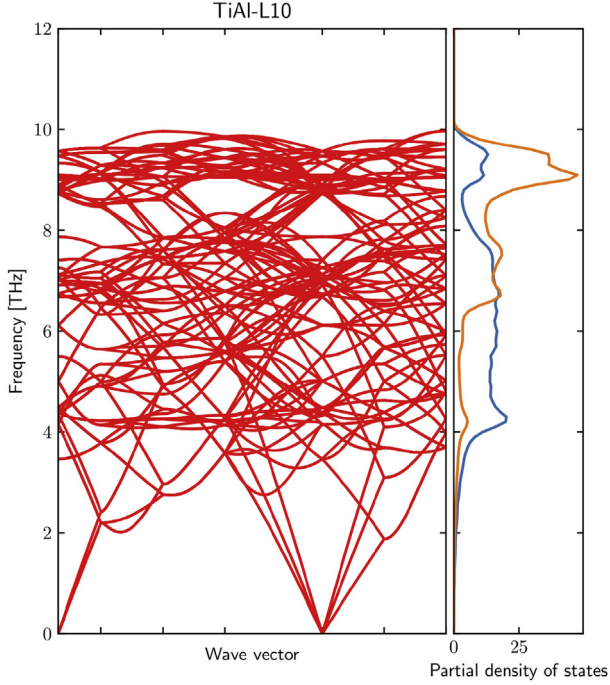


Fig. 3 – Phonon band structure (vBAND) and the projected density-of-states of TiAl-L1₀ of a 3 × 3 × 3 super-cell (54 atoms). Energies are expressed in THz. The phonon density-of-states is projected on atoms: the blue line corresponds to the vDOS of the Ti atom and the orange line corresponds to the Al atom. (For interpretation of the references to colour in this figure legend, the reader is referred to the Web version of this article.)

Understanding the effects associated with interface segregation requires first and foremost to understand what is happening inside the material. In particular, focus has been put on the infinite dilution solubility of hydrogen; for instance, vacancy-hydrogen interactions were not taken into consideration. The different positions in the L1₀ structure (space-group 123), where interstitial elements can be inserted, were identified: 1b, 1c, 2e, 2f, 2h, 4i, 4k, 4m, 4n, 4o and 8r Wyckoff positions. Atomic positions are given in Table 2 and most of them are displayed in Fig. 1. The L1₀ structure can be viewed as a bcc structure distorted along z. But the bcc structure only has one tetrahedral site and one octahedral site. Here, due to the symmetry break, it can be safely assumed that 1c and 2e sites are two distinct octahedral sites surrounded by four Ti atoms and two Al atoms, and that 1b and 2f sites are also two distinct octahedral sites, surrounded by four Al atoms and two Ti atoms. Regarding tetrahedral sites, there are three different positions: 4n, 4m and 4i sites. It can be noted that, contrary to what Chen [15] and Wang [17] concluded, there are more than two octahedral sites and one tetrahedral site. The insertion of interstitial elements in the TiAl-L1₀ system is thus more complex than expected.

Atomic positions and shapes of super-cells were fully relaxed, and insertion energies (E_i) of H atoms in interstitial sites were computed from different super-cell sizes ($2 \times 2 \times 2$, $3 \times 3 \times 3$ and $4 \times 4 \times 4$) to verify the accuracy and atomic

Table 2 – Wyckoff positions and site symmetry.

1b	1c	2e	2f
(0, 0, 1/2)	(1/2, 1/2, 0)	(0, 1/2, 1/2) (1/2, 0, 1/2)	(0, 1/2, 0) (1/2, 0, 0)
2h	4i	4m	4n
(1/2, 1/2, -z _i) (1/2, 1/2, z _i)	(0, 1/2, z _i) (1/2, 0, z _i) (0, 1/2, -z _i) (1/2, 0, -z _i)	(x _m , 0, 1/2) (-x _m , 0, 1/2) (0, x _m , 1/2) (0, -x _m , 1/2)	(x _n , 1/2, 0) (-x _n , 1/2, 0) (1/2, x _n , 0) (1/2, -x _n , 0)
4k	4o	8r	
(x _k , x _k , 1/2) (-x _k , -x _k , 1/2) (-x _k , x _k , 1/2) (x _k , -x _k , 1/2)	(x _o , 1/2, 1/2) (-x _o , 1/2, 1/2) (1/2, x _o , 1/2) (1/2, -x _o , 1/2)	(x _r , x _r , z _r) (-x _r , x _r , z _r) (-x _r , x _r , -z _r) (x _r , x _r , -z _r)	(-x _r , -x _r , z _r) (x _r , -x _r , z _r) (x _r , -x _r , -z _r) (-x _r , -x _r , -z _r)

positions of each configuration. This energy corresponds to the insertion energy at 0 K of H in the TiAl system. E_i is expressed by:

$$E_i = E_0[\text{TiAl} + \text{H}] - E_0[\text{TiAl}] - \frac{1}{2} E_0[\text{H}_2] \quad (1)$$

where $E_0[\text{TiAl} + \text{H}]$ and $E_0[\text{TiAl}]$ are the DFT energies of the super-cell, with and without hydrogen respectively. $E_0[\text{H}_2]$ is the DFT energy of the H₂ molecule (including spin effects). Final position energies are given in Table 3 for stable configurations only. Here, the effect the size of the super-cell is low; thus, from the small super-cells, the insertion energy is well converged.

After having minimized the forces (and stress), five stable positions were found: 1b, 1c, 2e, 2f and 4i. In the other configurations, hydrogen moves and relaxes in one of the five stable positions aforementioned. Results show that one of these configurations is nevertheless significantly lower in energy than the others: the 1c position with an insertion energy equal to -76 meV. It corresponds to the octahedral site composed of four Ti atoms and two Al atoms in the first-nearest neighboring positions. It is located on the top face of the unit-cell (along the c direction). It should correspond to the configuration found by Chen [15]. Our value agrees well with the value Chen found [15] (about -90 meV). The other positions on faces (2e) and edges (1b and 2f) of the super-cell box are less stable, at least 400 meV higher in energy than the 1c position. Wang's results [17] indicate that O₁ is more stable than O₂ (0.350 eV) and T

Table 3 – Formation energy (E_f , in eV), zero-point energy (H_v , in meV) and enthalpy of formation (H_f , in eV) of H atom in different “stable” configurations (see text).

	nb atom	1b	1c	2e	2f	4i
E_f	16	0.389	-0.069	0.974	0.869	z _i = 0.245 ₂ 0.220
	54	0.417	-0.078	0.934	0.861	0.232
	128	0.383	-0.076	0.871	0.828	0.226
H_v		-1	+14	unst.	unst.	+91
H_f		0.382	-0.062	-	-	0.317

(0.209 eV). As far as position is concerned, we can say that our results are in good agreement with Wang's.

To verify the stability of the sites, the inter-atomic constants (IFC) were computed from $3 \times 3 \times 3$ super-cells. When plotting frequencies along high symmetry points of the first Brillouin zone, two sites (2e and 2f) show two imaginary frequencies associated with H atoms, as can be seen in Fig. 4.

These positions are therefore dynamically unstable and can be identified as second-order transition states [21]. Verifications were conducted in order to make sure they occupy local maximums. These results will be helpful to reduce the number of possible jumps in the reasoning below. Therefore, only 1b, 1c and 4i positions are stable.

The zero-point energies (ZPE) of stable configurations, $H_v[H]$, were then computed from these IFC:

$$H_v[H] = F_v[\text{TiAl} + \text{H}] - F_v[\text{TiAl}] - \frac{1}{2} F_v[H_2] \quad (2)$$

where F_v are the Helmholtz free energies computed on fine \mathbf{q} -mesh grids using IFC, i.e.:

$$F_v = -k_B T \ln \mathcal{Z} = k_B T \sum_{\nu=1}^{3N} \int n_{\nu}(\mathbf{q}) \ln \left[2 \sinh \left(\frac{\hbar \omega_{\nu, \mathbf{q}}}{2k_B T} \right) \right] d\mathbf{q} \quad (3)$$

$\omega_{\nu, \mathbf{q}}$ are the frequencies in the wave vector \mathbf{q} and ν , the modes of the system. For the reference state, H_2 , $1/2F_v[H_2]$ is equal to 148 meV (the effect of temperature on the molecular partition function is neglected, see for instance [5,38]). Values are given in Table 3. It can be noted that the relative stability is unchanged and that the ZPE is low contrary to what is found in pure metals [4,20,39].

The phonon band structures and density-of-states of stable positions are displayed in Fig. 5.

Results show that the insertion of H atoms does not modify the phonon properties of the system, and that H frequencies are located at high energies (> 30 THz). From a numerical

standpoint, the solubility energy of H in TiAl (-0.062 eV, including the ZPE) is between that of H in Ti-hcp (-0.47 eV [20]) and that of H in Al-fcc ($+0.73$ eV [4,21]). In the reference states, Ti-H interactions are favored compared to Al-H interactions. When a hydrogen atom occupies a 1c site, it is surrounded by four Ti atoms, contrary to the configuration of the other sites. At 1c sites, H atoms in TiAl-L1₀ have a chemical environment similar to that of H atoms in the Ti-hcp system. The negative and low value of hydrogen H_f is in agreement with experimental observations [24,40]. This suggests that the solubility of hydrogen is low in the TiAl-L1₀ system.

In order to analyze the interactions between H atoms and the TiAl system, and to propose an explanation of the relative stability of H in 1c sites as compared to the other sites, the Bader charge (\mathcal{B}) [41], the charge transfer and the electronic density-of-states were computed. Values are listed in Table 4. Results show that there is a charge transfer from Al atoms to H atoms in all configurations. H atoms complete their s shells, they gain almost one e^- .

When a H atom is located in 1c, the charge transfer is smaller than in the others sites. This charge transfer can also be seen on the electronic density-of-states. The projected density-of-states on atoms of the TiAl-L1₀ structure for all stable configurations are displayed in Fig. 6. There is a strong similarity between eDOS if H is located either in a 1b or a 4i site: presence of a low energy peak (located around -9 eV) associated with the s shells of H, the p shells of Al and the s shells of Ti. Moreover, a hybridization can be noticed between H and Al states, in the range of $[-7; -6]$ eV, for 4i and 1c sites, but not for the 1b site. These results clarify the order of stability of these 3 sites.

The plot of the charge transfer $\Delta\rho$, Fig. 7, defined by:

$$\Delta\rho = \rho[\text{TiAl} + \text{H}] - \rho[\text{TiAl}] - \rho[\text{H}] \quad (4)$$

shows that the bonds are located between H atoms and Al atoms in first nearest-neighboring position as suggested by

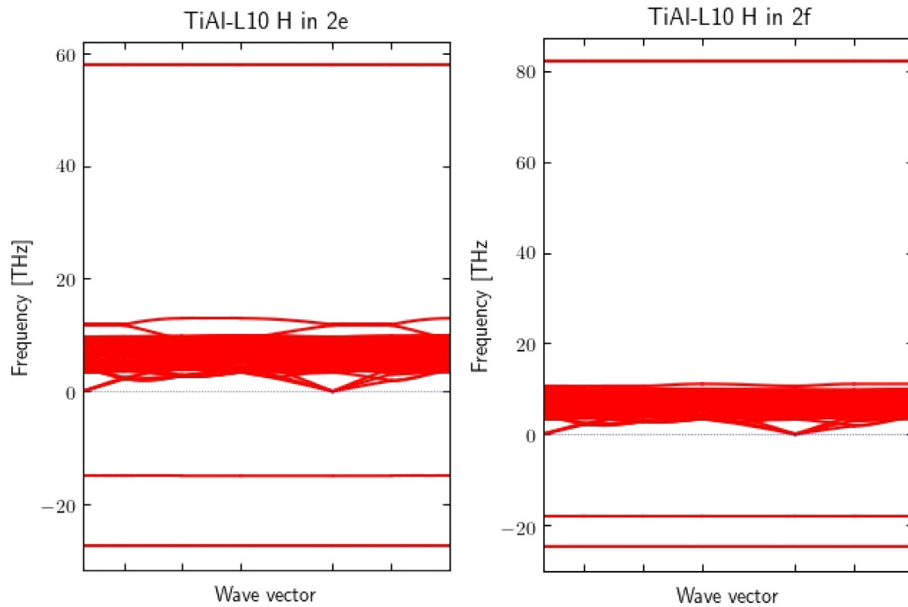


Fig. 4 – Vibrational band structure (vBAND) of H in 2e and 2f sites. In these cases, results show two imaginary frequencies (i.e., two negative frequencies). Energies are expressed in THz.

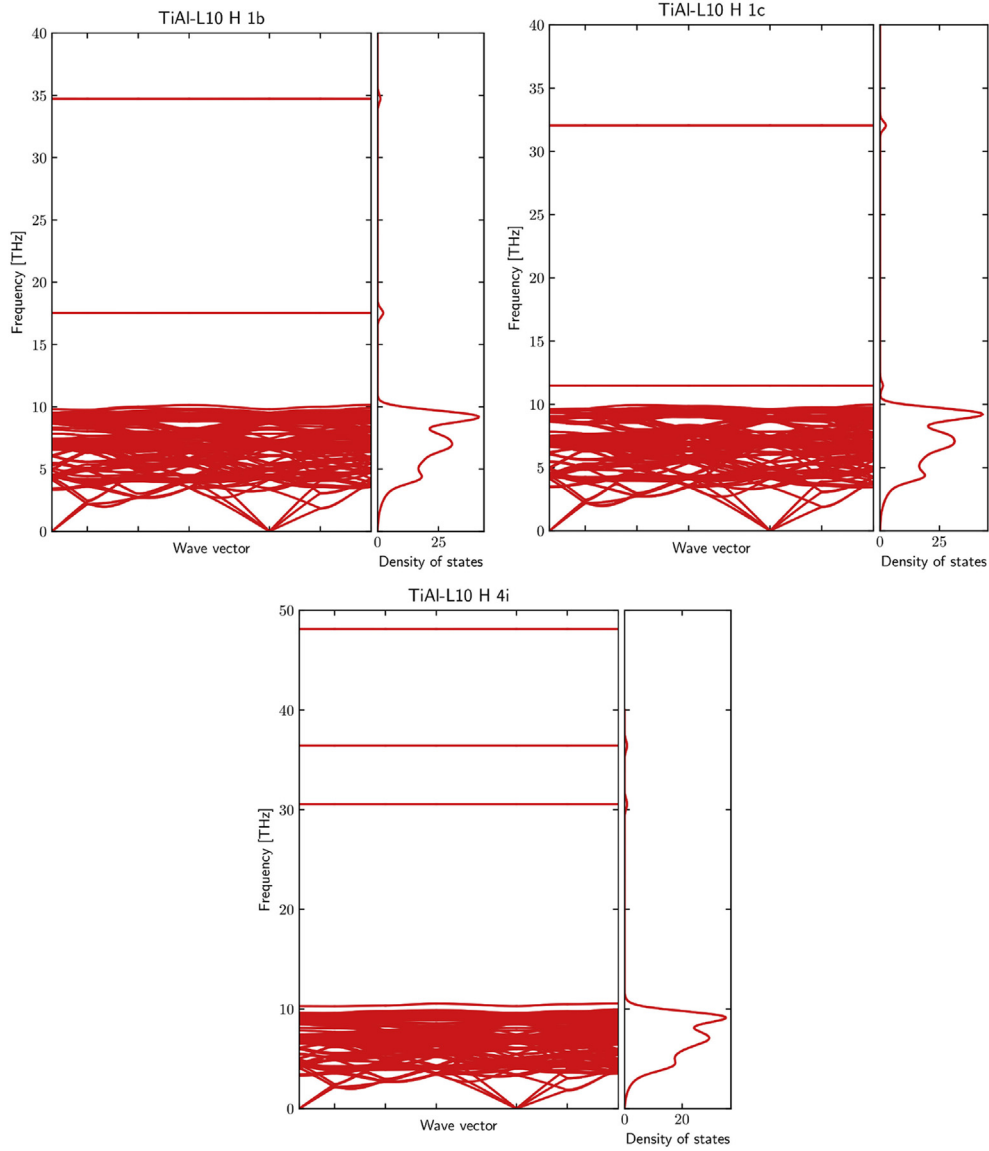


Fig. 5 – vBAND and density-of-states of H in 1b, 1c and 4i sites. Energies are expressed in THz.

Table 4 – Calculated values of the Bader charge (B , in e^-) of H atom, of Al atoms (in first-nearest neighboring position of the H atom) and of Ti atoms (in 1NN of the H atom) atoms, the volume of formation (Ω_f , in \AA^3), the volume difference between the empty and filled volume of Voronoï ($\delta \mathcal{V}_v$, in \AA^3) and the elastic dipoles (P_{ij} , in eV). The volume of Voronoï of the empty sites is equal to 8.11, 8.11 and 8.58 \AA^3 for 1b, 1c and 4i respectively. The number of electrons of each specie used in the pseudo-potential (labeled †), and the Bader charge of Al and Ti in TiAl-L1₀ (labeled ‡) are also given.

			1b	1c	4i
B	H	(1†)	2.1	1.9	2.0
	Al-1NN	(3‡, 3.7‡)	3.4	3.3	3.3
	Ti-1NN	(10‡, 9.3‡)	9.3	9.3	9.3
Ω_f		1.6	1.7	3.5	
$\delta \mathcal{V}_v$		0.24	0.31	0.80	
P_{ij}			$\begin{bmatrix} 1.9 & 0 & 0 \\ 0 & 1.9 & 0 \\ 0 & 0 & 0.2 \end{bmatrix}$	$\begin{bmatrix} 0.7 & 0 & 0 \\ 0 & 0.7 & 0 \\ 0 & 0 & 1.2 \end{bmatrix}$	$\begin{bmatrix} 2.3 & 0 & 0 \\ 0 & 2.3 & 0 \\ 0 & 0 & 2.0 \end{bmatrix}$

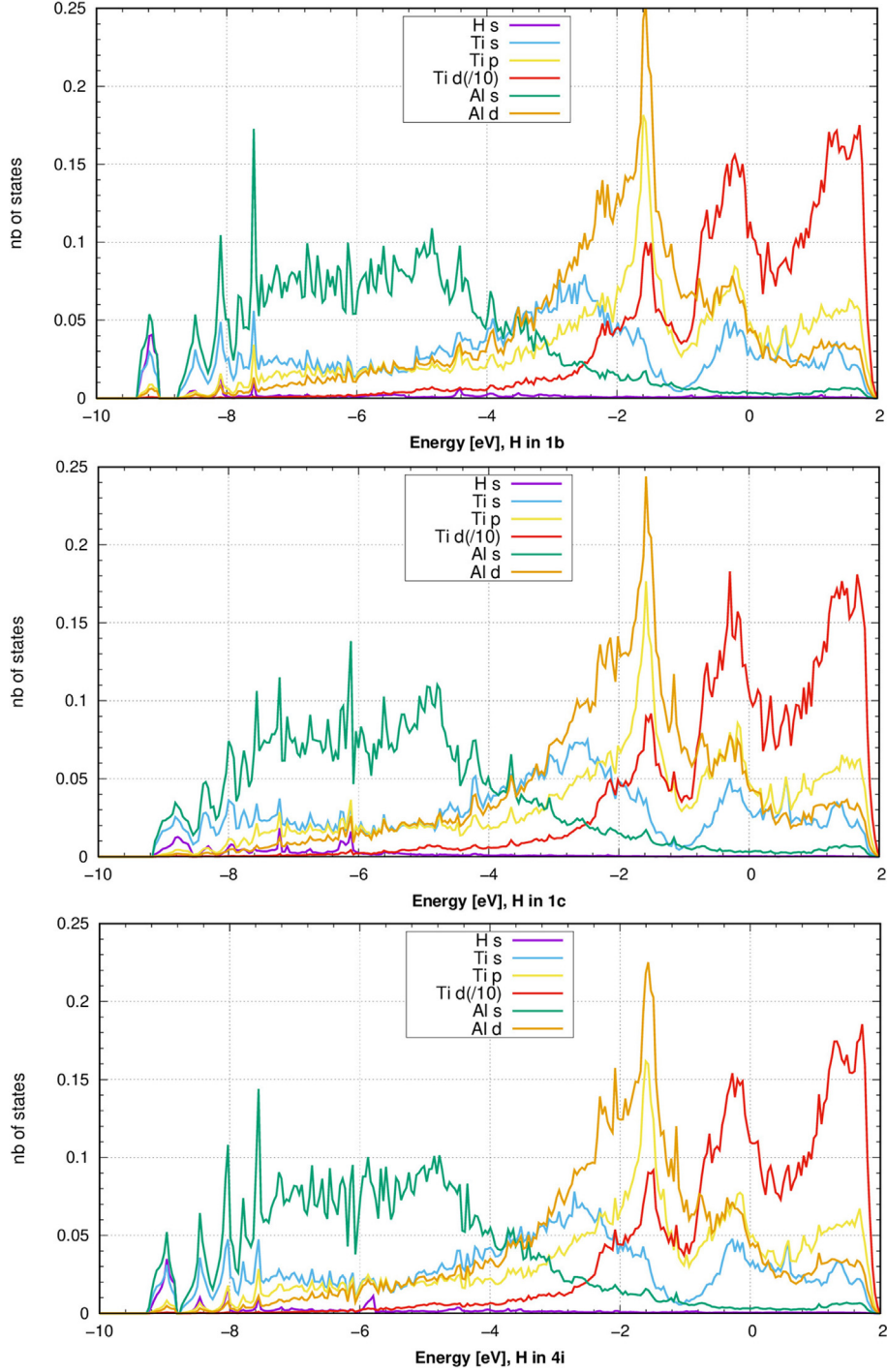


Fig. 6 – Projected density-of-states on atoms of the TiAl-L1₀ structure with a H atom in sites 1c, 1b and 4i.

the Bader analysis and electronic density-of-states. It can be noted that in the 1c configuration, the H atom attracts more strongly the electrons from its 1NN Ti and 1NN Al atoms, and form bonds with surrounding atoms. This is not the case in the other sites.

Both the volume of formation (Ω_f) and the volume of Voronoï were computed. Ω_f is given by:

$$\Omega_f = V[\text{TiAl} + \text{H}] - V[\text{TiAl}] \quad (5)$$

where $V[Y]$ is the volume of the super-cell with and without the H atom, and $\delta \mathcal{V}_v$:

$$\delta \mathcal{V}_v = \mathcal{V}[\text{TiAl} + \text{H}, V] - \mathcal{V}[\text{TiAl}, V] \quad (6)$$

where $\mathcal{V}[Y, V]$ are the volumes of Voronoï of the system Y calculated with and without hydrogen, computed with the same lattice parameters V . They characterize respectively the global and local steric effects. Both $\Omega_f \approx 1 \text{ \AA}^3$ and $\delta \mathcal{V}_v$ are relatively small. When H atoms are inserted in TiAl, the steric

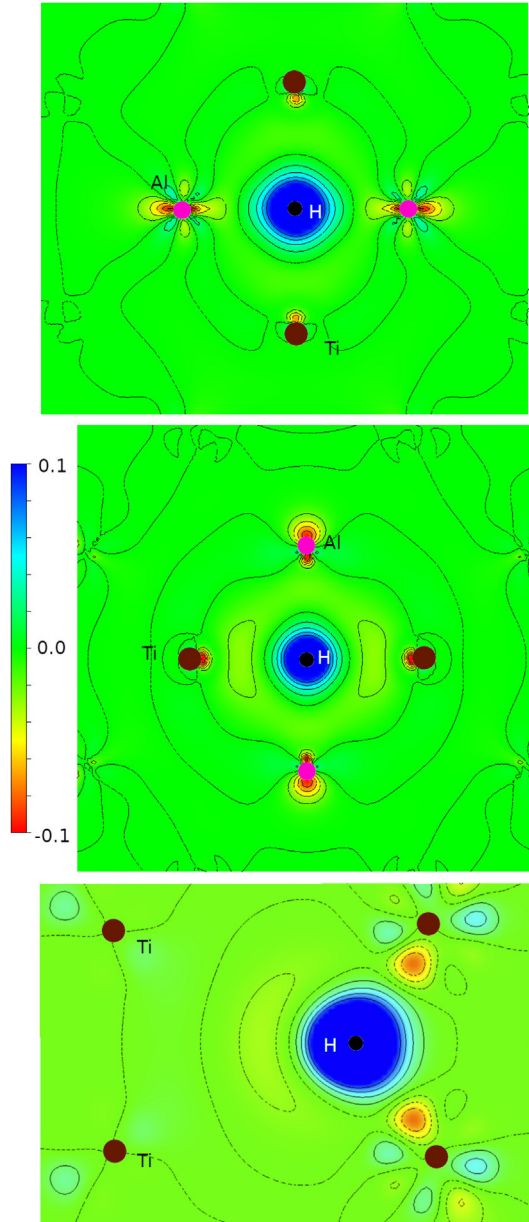


Fig. 7 – Contour maps of the charge transfer, $\Delta\rho$, when sites are filled: from top to bottom, H in 1b ((110) direction), 1c ((1-10) direction) and 4i ((100) direction) sites. Pink circles represent Al atoms, brown circles Ti atoms and black circles the H atom. (For interpretation of the references to colour in this figure legend, the reader is referred to the Web version of this article.)

effect on the system is only local. Both volumes indicate that hydrogen insertion only induces a local (but low) strain on the system.

Finally, we computed the elastic dipole tensors, P_{ij} , on $3 \times 3 \times 3$ super-cells with the same method used in Ref. [39] (the convention is here “+” for the system),

$$P_{ij} = V_0 \cdot \sigma_{ij} \quad (7)$$

Due to the symmetry of the system, diagonal components are not equivalent in all directions, just as C atoms in

iron [42,43]. Components are smallest ($<1.2\text{eV}$) in the case of 1c sites, elastic effects are thus minimal. It can be noted that both the steric effects and the electronic interactions have an influence on position stability. As a result, the insertion of H atoms only has a small and local impact on the TiAl system.

Hydrogen diffusivity

The diffusion mechanism will now be discussed. The main difficulty is to describe how H atoms can diffuse in an energy landscape such as the one generated by the TiAl crystal. Wang [17] studied the diffusion of H in TiAl. As explained previously, it is difficult to determine the exact position from his simulations. However, he studied two migration energies: between O_1 and O_2 sites, which is equal to about 0.91 eV, and between O_1 and T sites, about 0.21 eV. However, as stated below, several jumps are possible. Again, with no additional specifications, it is difficult to identify which jumps were studied.

In the discussion that follows, we only studied jumps between stable sites, i.e. between 1b, 1c and 4i sites. Eight paths were therefore examined, see Fig. 8 (the 1c-1c jump via 2f, in the (001) plan, is not represented).

NEB calculations [30] were conducted on $3 \times 3 \times 3$ super-cells so as to find the transition states. Five intermediate positions were used for each jump. After having identified a

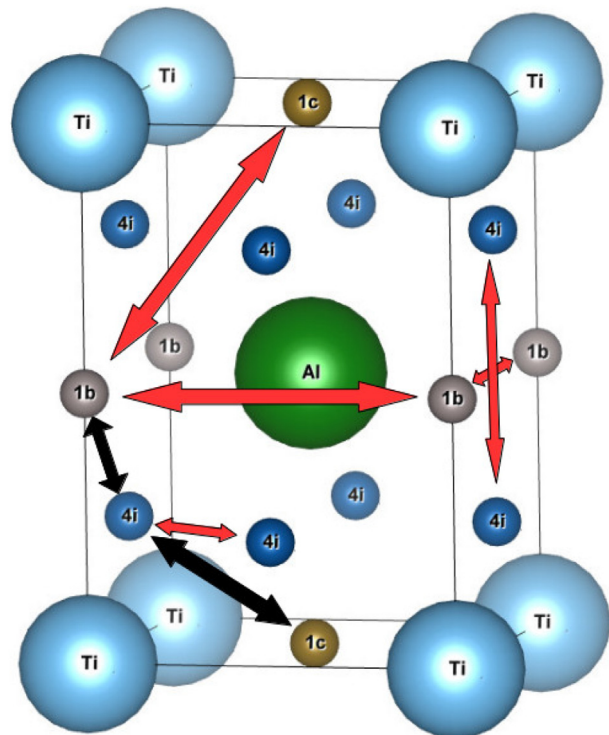


Fig. 8 – Representation of seven H-atom jumps between 1b, 1c and 4i sites: red arrows are “unacceptable” jumps (see text) and black arrows are “acceptable” jumps. (For interpretation of the references to colour in this figure legend, the reader is referred to the Web version of this article.)

transition state, its IFC was systematically computed in order to verify it and to calculate its attempt rate Γ_{xy} . The energy landscapes of the eight paths are depicted in Fig. 9.

Values are summarized in Table 5.

Firstly, results indicate that only three paths can be considered as acceptable jumps; indeed, some jumps are impossible due to the energy landscape of the TiAl-L1₀ structure. In the case of a direct jump between two first-nearest-neighbor 4i sites for instance, there is an intermediate stable position (1b). When a H atom in 4i wants to go to another 4i site through a 2e or a 2f site, NEB simulations show

that 2e and 2f sites are the transition states. As stated previously however, these sites have two imaginary frequencies (see Fig. 4), indicating that they are not first-order transition states. In the following, we thus ignore these possibilities. From phonon calculations, transition states were characterized so as to know whether they are of first-order or not. The transition state of 1b-1c is found to be a second-order transition state. *In fine*, only two acceptable jumps remain: the direct jump between 1c-4i sites and the one between 1b-4i sites. Upon leaving a 1c site, H atoms must go through a 4i site, which is significantly higher in energy (of at least 320 meV).

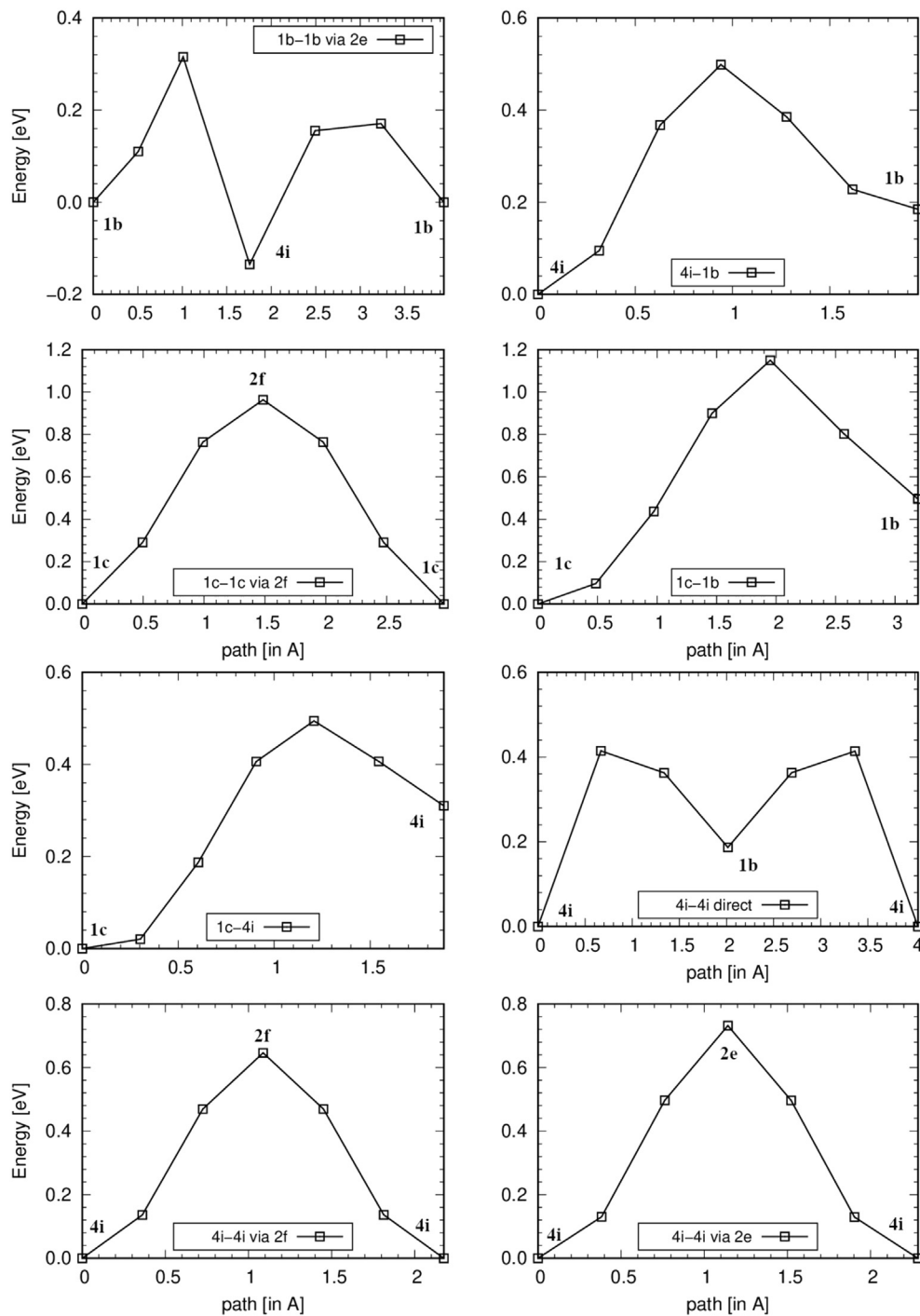


Fig. 9 – Eight NEB calculations for H atoms along different paths.

Table 5 – Migration energies (E_{x-y}^m , in eV) of jumps from x to y . Values marked with the † symbol are second-order transition states. Written in brackets is the position of the transition state, the numbers in bold correspond to the accepted jumps.

y/x	1b	1c	4i
1b	–	1.149†	0.498
1c	0.654†	0.963† [2f]	0.184
4i	0.314	0.494	0.732† [2e]/0.645† [2f]

For some (unacceptable) jumps, results indicate a high migration energy ranging from [0.96–1.14] eV. One of these values could correspond to the value found by Wang [17], which is 0.9 eV.

The quantum tunneling effects, as described by different authors in the literature [44,45], were neglected here. The tunneling effect is a correction to the classical diffusivity which has to be taken into account at low temperature (below ambient temperature). The study of hydrogen diffusion presented here is based on the theory commonly known as the semi-classical transition state theory. Moreover, the H diffusion is considered as a regular random walk, i.e., uncorrelated with respect to H jumps. The Eyring transition state theory [46] and the multi-states theory proposed by Landman [47,48] can now be used to examine diffusion coefficients. According to these theories, only first-order transition states were taken into consideration. Second-order transition states like 2e and 2f were left aside, the jump rates of these jumps are arguably negligible [21].

The characteristic quantity used to quantify the probability of leaving a site is the jump rate, Γ . It is computed by using the following equation:

$$\Gamma[T] = \frac{k_B T}{h} \frac{\mathcal{Z}_{TS}}{\mathcal{Z}_{Ei}} e^{-\Delta E_m/k_B T} \quad (8)$$

where ΔE_m corresponds to the (electronic) transition migration energy. \mathcal{Z}_{TS} is the (vibration) partition function for the transition state and \mathcal{Z}_{Ei} is the partition function for the initial position. \mathcal{Z} is expressed by eq. (3).

The diffusion coefficient (see Appendix A) can thus be expressed using Γ_{bi} , Γ_{ci} , Γ_{ib} and Γ_{ic} , where Γ_{xy} is the jump rate of a jump from an x site to a y site:

$$D_{x,y}[T] = a_0^2 \frac{\Gamma_{bi}\Gamma_{ci}(\Gamma_{ib} + \Gamma_{ic})}{4\Gamma_{bi}\Gamma_{ci} + \Gamma_{ci}\Gamma_{ib} + \Gamma_{bi}\Gamma_{ic}} \quad (9)$$

$$D_z[T] = 2c_0^2 \frac{\Gamma_{bi}\Gamma_{ci}\Gamma_{ib}\Gamma_{ic}}{(4\Gamma_{bi}\Gamma_{ci} + \Gamma_{ci}\Gamma_{ib} + \Gamma_{bi}\Gamma_{ic}) \cdot (\Gamma_{ib} + \Gamma_{ic})} \quad (10)$$

where a_0 and c_0 are the lattice parameters of the system. By combining eqs. (9) and (10), the ratio D_z/D_x is given by:

$$\frac{D_z}{D_x}[T] = 2 \cdot \left(\frac{c_0}{a_0}\right)^2 \cdot \frac{\Gamma_{ib}\Gamma_{ic}}{(\Gamma_{ib} + \Gamma_{ic})^2} \quad (11)$$

Using DFT values in eqs. (9) and (10), diffusion coefficients D_x and D_z were plotted as a function of temperature. They are displayed in Fig. 10.

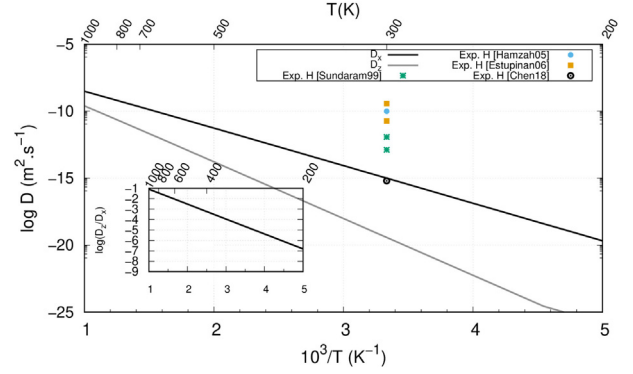


Fig. 10 – Diffusion coefficients of H atoms in TiAl, D_x , D_z and the ratio D_z/D_x (in log-scale), were plotted as a function of $1/T$. Experimental data, from Refs. [22–25], were added.

Table 6 – Activation energies (E_a in eV) and D_0 (in $10^{-6} \text{ m}^2/\text{s}$) obtained from an Arrhenius fit.

Direction	E_a	D_0
x, y	0.537	1.58
z	0.811	3.04

Diffusion coefficients were fitted with an Arrhenius law ($D[T] = D_0 \exp(-E_a/k_B T)$), to obtain D_0 and E_a , the activation energies. Parameters are reported in Table 6.

It can be noticed that, the diffusion in TiAl is strongly anisotropic, many orders of magnitude faster in the x and y planes than in the z direction. From a numerical standpoint, H atoms diffuse slower in TiAl than in many other metals [21]. For instance, these diffusion values are lower than those of H diffusion in pure polycrystalline titanium reported in the literature [20]. To reduce or enhance hydrogen diffusivity in metals, textured materials could be used.

Comparing these results to literature data is somewhat delicate. Five distinct values of H diffusivity in TiAl were found in the literature, always measured at room temperature. The values vary between $[3 \cdot 10^{-10}; 6 \cdot 10^{-16}] \text{ m}^2/\text{s}$ [22–25]. The only H diffusivity value found in the literature that matches the result obtained here is the one found by Chen [25], see Fig. 10, which corresponds to the slowest H diffusivity measured experimentally. In the present work, the ideal diffusion coefficient was computed from a bulk of γ -TiAl. However, the inherently complex microstructure of TiAl alloys (lamellar structure), the composition (many solute atoms, Nb, Cr, etc.) or the stoichiometry of Al and Ti atoms can vary from one experimental work to another. This could explain the important differences between all the values. For instance short-circuits of interfaces (grain boundaries, γ -TiAl/ α_2 -Ti $_3$ Al interfaces) could enhance H diffusivity in TiAl materials. All of these parameters could have enough impact to explain the discrepancy in the results obtained.

Conclusion

This work presents a complete study on the insertion and diffusion of hydrogen in the intermetallic TiAl-L1₀ system. It

was first demonstrated that hydrogen atoms in TiAl-L1₀ prefer occupy 1c octahedral sites. 1b and 4i sites were then identified as two additional stable configurations admitted by the system. However, their insertion energies are significantly higher than that of 1c sites. Based on electronic properties, charge transfers and elastic dipoles, it was concluded that 1c sites are more stable than the others. Distortion effects, both local (volumes of Voronoi) and long-ranged (volumes of formation and elastic dipoles) were quantified. The competition between elastic and electronic effects indicate a strong interaction between hydrogen and the metal.

Upon studying the diffusion of interstitial species, different paths were meticulously analyzed. Nevertheless, the explicit expressions of diffusivity given here take into account the different jumps. Results show that, in the TiAl-L1₀ system, hydrogen diffusion is slow and highly anisotropic.

Acknowledgments

This work was performed using HPC resources from CALMIP (Grant 2018-p0749). The author is grateful to A. Prillieux for his remarks and comments.

Appendix A. Multi-states model

In the case treated here, there are three stable sites (1b, 1c and 4i), but there is a limited number of possible jumps, D is expressed by (following Landman's method [47,48]):

$$D_{x,y}[T] = a_0^2 \frac{\Gamma_{bi}\Gamma_{ci}(\Gamma_{ib} + \Gamma_{ic})}{4\Gamma_{bi}\Gamma_{ci} + \Gamma_{ci}\Gamma_{ib} + \Gamma_{bi}\Gamma_{ic}} \quad (A.1)$$

$$D_z[T] = 2c_0^2 \frac{\Gamma_{bi}\Gamma_{ci}\Gamma_{ic}\Gamma_{ib}}{(4\Gamma_{bi}\Gamma_{ci} + \Gamma_{ci}\Gamma_{ib} + \Gamma_{bi}\Gamma_{ic}) \cdot (\Gamma_{ib} + \Gamma_{ic})} \quad (A.2)$$

This formula was obtained by first identifying the number of non-equivalent positions in the primitive cell. In this case, for H in the L1₀ system, there are six non-equivalent sites, labeled 1b, 1c and 4i_j, where $j \in [1, 4]$. Then, the different possible jumps from each sites were identified. Two quantities are thus required: the Laplace transform of the waiting time density matrix, $\underline{\psi}(u)$, and the Fourier transform matrix of the displacements of hydrogen in TiAl, $\underline{p}(k)$. $\underline{\psi}(u)$ is given by:

$$\underline{\psi}(u) = \begin{matrix} & 1b & 1c & 4i_1 & 4i_2 & 4i_3 & 4i_4 \\ \begin{matrix} 1b \\ 1c \\ 4i_1 \\ 4i_2 \\ 4i_3 \\ 4i_4 \end{matrix} & \begin{bmatrix} 0 & 0 & \frac{2\Gamma_{ib}}{K_i} & \frac{2\Gamma_{ib}}{K_i} & \frac{2\Gamma_{ib}}{K_i} & \frac{2\Gamma_{ib}}{K_i} \\ 0 & 0 & \frac{2\Gamma_{ic}}{K_i} & \frac{2\Gamma_{ic}}{K_i} & \frac{2\Gamma_{ic}}{K_i} & \frac{2\Gamma_{ic}}{K_i} \\ \frac{2\Gamma_{bi}}{K_b} & \frac{2\Gamma_{ci}}{K_c} & 0 & 0 & 0 & 0 \\ \frac{2\Gamma_{bi}}{K_b} & \frac{2\Gamma_{ci}}{K_c} & 0 & 0 & 0 & 0 \\ \frac{2\Gamma_{bi}}{K_b} & \frac{2\Gamma_{ci}}{K_c} & 0 & 0 & 0 & 0 \\ \frac{2\Gamma_{bi}}{K_b} & \frac{2\Gamma_{ci}}{K_c} & 0 & 0 & 0 & 0 \end{bmatrix} \end{matrix} \quad (A.3)$$

where $K_b = 8\Gamma_{bi} + u$, $K_c = 8\Gamma_{ci} + u$ and $K_i = 2\Gamma_{ib} + 2\Gamma_{ic} + u$. Γ_{xy} is the probability of escape from internal state x to another state y . $\underline{p}(k)$ is given by:

$$\underline{p}(k) = \begin{matrix} & 1b & 1c & 4i_1 & 4i_2 & 4i_3 & 4i_4 \\ \begin{matrix} 1b \\ 1c \\ 4i_1 \\ 4i_2 \\ 4i_3 \\ 4i_4 \end{matrix} & \begin{bmatrix} 0 & 0 & A_{i_1b} & A_{i_2b} & A_{i_3b} & A_{i_4b} \\ 0 & 0 & A_{i_1c} & A_{i_2c} & A_{i_3c} & A_{i_4c} \\ A_{bi_1} & A_{ci_1} & 0 & 0 & 0 & 0 \\ A_{bi_2} & A_{ci_2} & 0 & 0 & 0 & 0 \\ A_{bi_3} & A_{ci_3} & 0 & 0 & 0 & 0 \\ A_{bi_4} & A_{ci_4} & 0 & 0 & 0 & 0 \end{bmatrix} \end{matrix} \quad (A.4)$$

Where

$$\begin{matrix} A_{i_1b} = [1 + e^{i l_x k_x}] / 2 \\ A_{i_1c} = [1 + e^{-i l_y k_y}] / 2 \\ A_{i_2b} = [1 + e^{i l_y k_y}] / 2 \\ A_{i_2c} = [1 + e^{-i l_x k_x}] / 2 \\ A_{i_3b} = [1 + e^{i l_x k_x}] / 2 \\ A_{i_3c} = e^{i l_z k_z} [1 + e^{-i l_y k_y}] / 2 \\ A_{i_4b} = [1 + e^{i l_y k_y}] / 2 \\ A_{i_4c} = e^{i l_z k_z} [1 + e^{-i l_x k_x}] / 2 \end{matrix} \left\| \begin{matrix} A_{bi_1} = [1 + e^{-i l_x k_x}] / 2 \\ A_{ci_1} = [1 + e^{i l_y k_y}] / 2 \\ A_{bi_2} = [1 + e^{-i l_y k_y}] / 2 \\ A_{ci_2} = [1 + e^{i l_x k_x}] / 2 \\ A_{bi_3} = [1 + e^{-i l_x k_x}] / 2 \\ A_{ci_3} = e^{-i l_z k_z} [1 + e^{i l_y k_y}] / 2 \\ A_{bi_4} = [1 + e^{-i l_y k_y}] / 2 \\ A_{ci_4} = e^{-i l_z k_z} [1 + e^{i l_x k_x}] / 2 \end{matrix} \right. \quad (A.5)$$

with $l_x = l_x = a_0$ and $l_z = c_0$. In order to derive D_{xy} and D_z , the procedure suggested by Landmann [48] was then used.

REFERENCES

- [1] Jabbar H, Monchoux J-P, Thomas M, Couret A. Microstructures and deformation mechanisms of a g4 tial alloy produced by spark plasma sintering. Acta Mater 2011;59(20):7574–85. <https://doi.org/10.1016/j.actamat.2011.09.001>. <http://www.sciencedirect.com/science/article/pii/S1359645411006288>.
- [2] Murr L, Gaytan S, Ceylan A, Martinez E, Martinez J, Hernandez D, Machado B, Ramirez D, Medina F, Collins S, Wicker R. Characterization of titanium aluminide alloy components fabricated by additive manufacturing using electron beam melting. Acta Mater 2010;58(5):1887–94. <https://doi.org/10.1016/j.actamat.2009.11.032>. <http://www.sciencedirect.com/science/article/pii/S1359645409008118>.
- [3] Chen Y, Yue H, Wang X, Xiao S, Kong F, Cheng X, Peng H. Selective electron beam melting of tial alloy: microstructure evolution, phase transformation and microhardness. Mater Char 2018;142:584–92. <https://doi.org/10.1016/j.matchar.2018.06.027>. <http://www.sciencedirect.com/science/article/pii/S1044580318309173>.
- [4] Wolverton C, Ozolins V, Asta M. Hydrogen in aluminum: first-principles calculations of structure and thermodynamics. Phys Rev B 2004;69:144109. <https://doi.org/10.1103/PhysRevB.69.144109>.
- [5] Fernandez N, Ferro Y, Kato D. Hydrogen diffusion and vacancies formation in tungsten: density functional theory calculations and statistical models. Acta Mater 2015;94:307–18. <https://doi.org/10.1016/j.actamat.2015.04>.

052. <http://www.sciencedirect.com/science/article/pii/S1359645415003043>.
- [6] David M, Connétable D. Diffusion of interstitials in metallic systems, illustration of a complex study case: aluminum. *J Phys Condens Matter* 2017;29(45):455703. <http://stacks.iop.org/0953-8984/29/i=45/a=455703>.
- [7] Fuhe W, Chongyu W. First-principles investigation of hydrogen embrittlement in polycrystalline Ni_{3}Al . *Phys Rev B* 1998;57:289–95. <https://doi.org/10.1103/PhysRevB.57.289>.
- [8] Johnson DF, Carter EA. First-principles assessment of hydrogen absorption into Fe and Fe₃Si: towards prevention of steel embrittlement. *Acta Mater* 2010;58(2):638–48. <https://doi.org/10.1016/j.actamat.2009.09.042>. <http://www.sciencedirect.com/science/article/pii/S135964540900648X>.
- [9] Geng WT, Freeman AJ, Wu R, Geller CB, Reynolds JE. Embrittling and strengthening effects of hydrogen, boron, and phosphorus on a $\Sigma 5$ nickel grain boundary. *Phys Rev B* 1999;60:7149–55. <https://doi.org/10.1103/PhysRevB.60.7149>.
- [10] Shen X, Connétable D, Tanguy D. Modeling segregation of hydrogen to the σ_{h} –(221)–[110] symmetric tilt grain boundary in Al. *Phil Mag* 2014;94:2247–61.
- [11] Martin ML, Dadfarnia M, Nagao A, Wang S, Sofronis P. Enumeration of the hydrogen-enhanced localized plasticity mechanism for hydrogen embrittlement in structural materials. *Acta Mater* 2019;165:734–50. <https://doi.org/10.1016/j.actamat.2018.12.014>. <http://www.sciencedirect.com/science/article/pii/S135964541830956X>.
- [12] Fukai Y, Shizuku Y, Kurokawa Y. *J Alloy Comp* 2001;329:195–201.
- [13] Nazarov R, Hickel T, Neugebauer J. Ab initio study of h-vacancy interactions in fcc metals: implications for the formation of superabundant vacancies. *Phys Rev B* 2014;89:144108. <https://doi.org/10.1103/PhysRevB.89.144108>.
- [14] Tanguy D, Wang Y, Connétable D. Stability of vacancy-hydrogen clusters in nickel from first principles calculations. *Acta Mater* 2014;78:135–43.
- [15] Chen S, Liang C, Gong H. Structural stability, mechanical property and elastic anisotropy of tial-h system. *Int J Hydrogen Energy* 2012;37(3):2676–84. 2010 AIChE Annual Meeting Topical Conference on Hydrogen Production and Storage Special Issue, <https://doi.org/10.1016/j.ijhydene.2011.11.025>. <http://www.sciencedirect.com/science/article/pii/S0360319911025237>.
- [16] Wei Y, Zhang Y, Lu G, Xu H. A first-principles study of site occupancy and interfacial energetics of an h-doped tial-ti3al alloy. *Sci China Phys Mech Astron* 2012;55(2):228–34. <https://doi.org/10.1007/s11433-011-4600-x>.
- [17] Wang JW, Gong H. Effect of hydrogen concentration on various properties of gamma tial. *Int J Hydrogen Energy* 2014;39(4):1888–96. <https://doi.org/10.1016/j.ijhydene.2013.11.045>. <http://www.sciencedirect.com/science/article/pii/S0360319913027705>.
- [18] Jiang C, Wolverton C, Sofo J, Chen L, Liu Z. *Phys Rev B* 2004;69:214202.
- [19] Wimmer E, Wolf W, Sticht J, Saxe P, Geller CB, Najafabadi R, Young GA. Temperature-dependent diffusion coefficients from ab initio computations: hydrogen, deuterium, and tritium in nickel. *Phys Rev B* 2008;77:134305. <https://doi.org/10.1103/PhysRevB.77.134305>.
- [20] Connétable D, Huez J, Andrieu E, Mijoule C. First-principles study of the migration process of hydrogen and vacancy in titanium. *J Phys: Condens Matter* 2011;23:405401. <https://doi.org/10.1088/0953-8984/23/40/405401>.
- [21] Connétable D, David M. Diffusion of interstitial species (h and o atoms) in fcc systems (Al, Cu, Co, Ni and Pd): contribution of first and second order transition states. *J Alloy Comp* 2019;772:280–7. <https://doi.org/10.1016/j.jallcom.2018.09.042>. <http://www.sciencedirect.com/science/article/pii/S0925838818332717>.
- [22] Sundaram P, Wessel E, Ennis P, Quadackers W, Singheiser L. Diffusion coefficient of hydrogen in a cast gamma titanium aluminide. *Scripta Mater* 1999;41(1):75–80. [https://doi.org/10.1016/S1359-6462\(99\)00056-1](https://doi.org/10.1016/S1359-6462(99)00056-1). <http://www.sciencedirect.com/science/article/pii/S1359646299000561>.
- [23] Hamzah E, Suardi K, Ourdjini A. Effect of microstructures on the hydrogen attack to gamma titanium aluminide at low temperature. *Mater Sci Eng* 2005;397(1):41–9. <https://doi.org/10.1016/j.msea.2005.01.054>. <http://www.sciencedirect.com/science/article/pii/S0921509305000651>.
- [24] Estupiñan H, Uribe I, Sundaram P. Hydrogen permeation in gamma titanium aluminides. *Corros Sci* 2006;48(12):4216–22. <https://doi.org/10.1016/j.corsci.2006.04.010>. <http://www.sciencedirect.com/science/article/pii/S0010938X0600151X>.
- [25] Chen Y, Zhang T, Song L. Hydride formation during cathodic charging and its effect on mechanical properties of a high Nb containing TiAl alloy. *Int J Hydrogen Energy* 2018;43(16):8161–9. <https://doi.org/10.1016/j.ijhydene.2018.03.073>. <http://www.sciencedirect.com/science/article/pii/S0360319918308346>.
- [26] Kresse G, Hafner J. Ab initio molecular dynamics for liquid metals. *Phys Rev B* 1993;47:558–61. <https://doi.org/10.1103/PhysRevB.47.558>.
- [27] Perdew JP, Burke K, Ernzerhof M. Generalized gradient approximation made simple. *Phys Rev Lett* 1996;77:3865–8. <https://doi.org/10.1103/PhysRevLett.77.3865>.
- [28] Kresse G, Joubert D. From ultrasoft pseudopotentials to the projector augmented-wave method. *Phys Rev B* 1999;59:1758–75. <https://doi.org/10.1103/PhysRevB.59.1758>.
- [29] Monkhorst HJ, Pack JD. Special points for Brillouin-zone integrations. *Phys Rev B* 1976;13:5188–92. <https://doi.org/10.1103/PhysRevB.13.5188>.
- [30] Henkelman G, Uberuaga BP, Jónsson H. A climbing image nudged elastic band method for finding saddle points and minimum energy paths. *The Journal of Chemical Physics* 2000;113(22):9901–4. <https://doi.org/10.1063/1.1329672>. arXiv:..
- [31] Togo A, Oba F, Tanaka I. First-principles calculations of the ferroelastic transition between rutile-type and CaCl₂-type SiO₂ at high pressures. *Phys Rev B* 2008;78:134106. <https://doi.org/10.1103/PhysRevB.78.134106>.
- [32] Banumathy S, Ghosal P, Singh A. On the structure of the TiAl phase in Ti–Al and Ti–Al–Nb alloys. *J Alloy Comp* 2005;394(1):181–5. <https://doi.org/10.1016/j.jallcom.2004.10.029>. <http://www.sciencedirect.com/science/article/pii/S0925838804013751>.
- [33] Tanaka K. Single-crystal elastic constants of gamma-TiAl. *Phil Mag Lett* 1996;73(2):71–8. <https://doi.org/10.1080/095008396181019>. arXiv:..
- [34] First principles calculations of elastic properties of metals.
- [35] He Y, Schwarz R, Migliori A, Whang S. Elastic constants of single crystal gamma-TiAl. *J Mater Res* 1995;10(5):1187–95. <https://doi.org/10.1557/JMR.1995.1187>.
- [36] Kittel C. *Introduction to solid state physics*. New York: Wiley; 1996.
- [37] Fisher ES, Renken CJ. Single-crystal elastic moduli and the hcp → bcc transformation in Ti, Zr, and Hf. *Phys Rev* 1964;135:A482–94. <https://doi.org/10.1103/PhysRev.135.A482>.
- [38] D. Matthieu, M. Daniel, C. Damien, Insertion and diffusion of interstitial atoms (h, c, n and o) in nickel, [submitted].
- [39] Connétable D, David M. Study of vacancy-(h, b, c, n, o) Clusters in Al using DFT and statistical approach: consequences on solubility of solutes. *J Alloy Comp* 2018;748:12–25. <https://doi.org/10.1016/j.jallcom.2018.03.081>. <http://www.sciencedirect.com/science/article/pii/S0925838818309423>.

- [40] Hashi K, Ishikawa K, Suzuki K, Aoki K. Hydrogen absorption and desorption in the binary Ti–Al system. *J Alloy Comp* 2002;330–332:547–50. [https://doi.org/10.1016/S0925-8388\(01\)01660-7](https://doi.org/10.1016/S0925-8388(01)01660-7). <http://www.sciencedirect.com/science/article/pii/S0925838801016607>.
- [41] Henkelman G, Arnaldsson A, Jónsson H. A fast and robust algorithm for bader decomposition of charge density. *Comput Mater Sci* 2006;36(3):354–60. <https://doi.org/10.1016/j.commatsci.2005.04.010>. <http://www.sciencedirect.com/science/article/pii/S0927025605001849>.
- [42] Clouet E, Garruchet S, Nguyen H, Perez M, Becquart CS. Dislocation interaction with c in alpha-fe: a comparison between atomic simulations and elasticity theory. *Acta Mater* 2008;56(14):3450–60. <https://doi.org/10.1016/j.actamat.2008.03.024>. <http://www.sciencedirect.com/science/article/pii/S1359645408002218>.
- [43] Maugis P, Chentouf S, Connétable D. Stress-controlled carbon diffusion channeling in bct-iron: a mean-field theory. *J Alloy Comp* 2018;769:1121–31. <https://doi.org/10.1016/j.jallcom.2018.08.060>. <http://www.sciencedirect.com/science/article/pii/S0925838818329335>.
- [44] Sundell PG, Wahnström G. Activation energies for quantum diffusion of hydrogen in metals and on metal surfaces using delocalized nuclei within the density-functional theory. *Phys Rev Lett* 2004;92:155901. <https://doi.org/10.1103/PhysRevLett.92.155901>.
- [45] Di Stefano D, Mrovec M, Elsässer C. First-principles investigation of quantum mechanical effects on the diffusion of hydrogen in iron and nickel. *Phys Rev B* 2015;92:224301. <https://doi.org/10.1103/PhysRevB.92.224301>.
- [46] Eyring H. The activated complex in chemical reactions. *J Chem Phys* 1935;3(2):107–15. <https://doi.org/10.1063/1.1749604>. arXiv:.
- [47] Landman U, Shlesinger MF. Stochastic theory of multistate diffusion in perfect and defective systems. i. mathematical formalism. *Phys Rev B* 1979;19:6207–19. <https://doi.org/10.1103/PhysRevB.19.6207>.
- [48] Landman U, Shlesinger MF. Stochastic theory of multistate diffusion in perfect and defective systems. ii. case studies. *Phys Rev B* 1979;19:6220–37. <https://doi.org/10.1103/PhysRevB.19.6220>.